LANDSAT 9 THERMAL INFRARED SENSOR 2 SPECTRAL RESPONSE TEST: UPDATES AND PERSPECTIVE

Aaron J. Pearlman[1], Boryana Efremova[1], Allen Lunsford[2], Joel McCorkel[3], and Dennis Reuter[3]

[1]GeoThinkTank LLC, Washington DC 20009, USA
[2] Catholic University of America, Washington DC 20064, USA
[3] NASA Goddard Space Flight Center, Greenbelt, MD 20771, USA

ABSTRACT

The Thermal Infrared Sensor 2 (TIRS-2) that will fly aboard Landsat 9 has undergone pre-launch spectral characterization to demonstrate that its spectral response requirements will be met with few waivers. The test was conducted both at the subsystem level and, after upgrading the test setup and improving the alignment methodology, at instrument-level as well. This work reviews these upgrades and alignment methodology that contributed to a reduction in spectral response uncertainties to a relatively small value relative to the overall TIRS-2 radiometric uncertainty requirements. The spectral response results show an increase in signal to noise ratio and reference detector stability from subsystem-level measurements. Spectral response testing is part of a comprehensive pre-launch test program that ensures TIRS-2 will achieve the performance necessary for a variety of environmental applications.

1. INTRODUCTION

The Thermal Infrared Sensor-2 (TIRS-2) to be integrated on Landsat 9 is scheduled to launch at the end of 2020 to continue the Landsat Program's legacy of providing moderate resolution thermal imagery [1, 2, 3]. Scientists use the imagery for a wide variety of environmental applications like assessing evapotranspiration through land surface temperature retrievals. Its two bands, at 10.8 μm and 12 μm, enable more accurate retrievals than using the single channel available prior to Landsat 8 [4]. The instrument is a pushbroom sensor with a 15° cross-track field of view with the same basic architecture as TIRS but with some improvements such as increased redundancy and improved stray light suppression. It has a f/1.6 four-lens telescope that focuses onto quantum well infrared detector (QWIP) arrays ([5]), an on-board blackbody for calibration, and a scene-select mirror for switching between Earth view, blackbody, and space views.

TIRS-2 has been undergoing a comprehensive pre-launch calibration testing campaign to evaluate its spectral, geometric, and radiometric performance. Last year, TIRS-2 Imaging Performance and Cryoshell Evaluation (TIPCE) test campaign was conducted to evaluate the relative spectral response (RSR) as well as several other performance characteristics - optical stray light effects, optical focus of the telescope, and spatial performance. The TIPCE configuration includes the major instrument components (flight focal plane assembly, filters, and telescope), but not the full instrument (e.g. it does not include the scene select mirror). Thus, it served as a useful baseline for spectral performance and provided a reliable first estimate of the instrument-level RSR and uncertainties.

The spectral testing campaign continued with the instrument-level spectral response characterization test earlier this year to measure its performance including the RSR of the full TIRS-2 instrument -– scene select mirror, telescope optics, filters, and detectors – in flight-like conditions and verify the compliance to the instrument requirements. Based on the results from the TIPCE measurements, we implemented several improvements to decrease the uncertainty of the measurements before instrument-level testing. This paper describes the system improvements, their implementation, and results.

2. SPECTRAL CHARACTERIZATION TEST DESCRIPTION

TIRS-2 pre-launch measurements – including radiometric, geometric, and spectral performance testing – are taken with the calibration ground support equipment (GSE) (Fig. 1). The calibration GSE has a special mode designed for spectral measurements where the internal blackbody targets used for radiometric tests are bypassed so that a beam from the monochromator-based setup outside the thermal vacuum chamber can propagate through it and onto the sensor. The monochromator setup consists of a blackbody at $1000\,^\circ C$ as a source filling the entrance slit of a monochromator (with 50 l/mm grating with blaze wavelength of 12 μm, and reciprocal dispersion 78.3 nm/mm). The monochromator output is collimated and directed into the chamber through a ZnSe window, where it is directed into the TIRS-2 aperture by the calibration GSE optics. Outside the chamber, as shown in Fig. 1 a flip mirror can redirect the monochromator beam to a liquid nitrogen-cooled HgCdTe detector used as a radiance monitor. In this configuration, the blackbody signal is chopped so that it can be retrieved in the presence of large ambient background with a lock-in amplifier.

The calibration GSE is comprised of optics to focus and recollimate the beam in order to fill the TIRS-2 telescope aperture. It also has a steering mirror placed on a translation stage with azimuth and elevation adjustments to direct the beam to any location on the three detector arrays. The illumination through the monochromator slits cover a few ($\sim$ 10) of the 640 science row pixels per detector array at a time. Several locations distributed along the arrays are observed in order to characterize any instrument-level low frequency spatial variations of the RSR shape.

During the spectral shape test, the TIRS-2 instrument is commanded to read twelve rows for each spectral channel for the three QWIP detector arrays as opposed to its science read-out mode

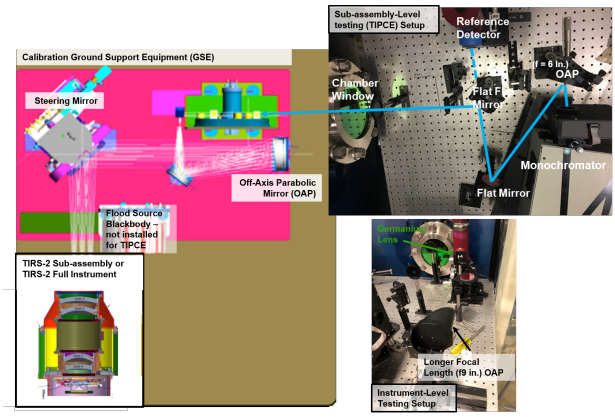

Figure 1: Sub-assembly testing (TIPCE) and instrument-level spectral setup. *Top Right*: The monochromator setup outside the thermal vacuum chamber where a blackbody signal propagates through the monochromator and is collimated and directed to either the chamber window or to a reference detector. *Bottom Right*: The updated monochromator setup for instrument-level testing including a longer focal length OAP and germanium coupling lens for the reference detector. *Left*: The calibration GSE provides additional optics inside the chamber to direct to the TIRS-2 subassembly or full instrument.

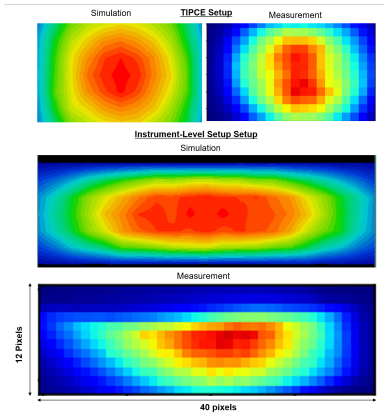

Figure 2: *Top* A modeled TIRS-2 slit image with the TIPCE setup and a sample measured TIRS-2 slit image taken during TIPCE. *Center/Bottom*: A modeled and measured TIRS-2 slit image with the instrument-level setup.

when it is reading only two rows per channel. The 12-row reading pattern facilitates centering the slit image onto the science rows, and allows us to account for test artifacts observed over the slit image (e.g. effects from dispersion across the slit, defocusing, etc.). The spectral measurements are collected to cover the in-band region for both spectral channels at 0.05 μm wavelength step. At each wavelength step, TIRS-2 collects 100 samples of the blackbody, followed by 100 shuttered samples used to estimate and subtract the thermal background. The background subtracted TIRS-2 digital numbers (dn) are then corrected using the HgCdTe reference detector measurements (V_{ref}) to account for the blackbody source spectral shape as well any spectral dependence of the monochromator optics transmittances and other optical elements in the common optical path of the HgCdTe detector and TIRS-2. The spectral dependence of the chamber window and calibration GSE optics transmittances are also accounted for ($\tau_{TIRS\,path}$), as are the transmittances of optical components specific to the reference detector optical path ($\tau_{ref\,path}$).

$$dn_{corr}(\lambda, pix) = \frac{dn_{TIRS}(\lambda, pix)\tau_{ref\,path}}{\tau_{TIRS\,path} V_{ref}}.$$

Finally the RSR is constructed for each pixel of each location by normalizing the corrected dn_{corr} values to their maximum:

$$RSR_{TIRS}(\lambda, pix) = \frac{dn_{corr}(\lambda, pix)}{max_{\lambda}(dn_{corr}(\lambda, pix)}.$$

The TIPCE and instrument-level data set contains individual RSRs for all illuminated pixels of each location – a total of 18 locations for TIPCE and 30 locations for instrument-level per spectral channel (three or five locations per detector array). The TIPCE results show that the RSR variability across the slit image per location is most likely driven by the test setup and not the intrinsic differences on a per-pixel level [6]. The dispersion across the slit can not completely explain the shape variation and is probably the result of defocusing and the angular dependence of the QWIP response. This was the motivation behind improving the alignment and collimation for instrument-level testing, so that the variation across the slit would be dominated by the dispersion only.

From the TIPCE results, we also sought to boost the signal and SNR by increasing transmission (reducing vignetting) through the calibration GSE and increase the stability of the reference detector measurement, since it did not have the ability to discern any potential source radiance drift. We will discuss how these improvements and the other uncertainty contributions affected the overall instrument-level spectral response uncertainty.

3. OPTICAL SETUP UPGRADES AND VERIFICATION

In order to increase the throughput of the calibration GSE, we replaced the 6-inch focal length OAP with one having a longer focal length (9 inches) in the monochromator setup. The impact of this change was estimated using an optical model that accounts for the blackbody's Lambertian illumination and all apertures within the system. The qualitative agreement in shape and size between measured and simulated images are shown in Fig. 2 for both OAPs corresponding to sub-assembly and instrument-level testing setups. The figure also shows the longer OAP yields a more slit-like shape. Note that the slit width was reduced for instrument-level testing to increase the resolution. The measured slit image appears cut off due to the imperfect centering of image on the 12-rows that are read out.

This new OAP was integrated with an improved alignment/ collimation methodology using a combination of shear plate interferometry and slit image analysis using visible sources. A laser placed at the output slit was collimated with the OAP with the aid of the shear plate interferometer. Once the shear plate showed fringes in the appropriate direction (ie. the beam was collimated), the laser source was replaced by a high intensity lamp at the input of the monochromator to more accurately simulate the blackbody input configuration. A visible camera with its focus at infinity several meters away viewed the output of the OAP while adjusting its distance from the output slit. The distance of highest contrast

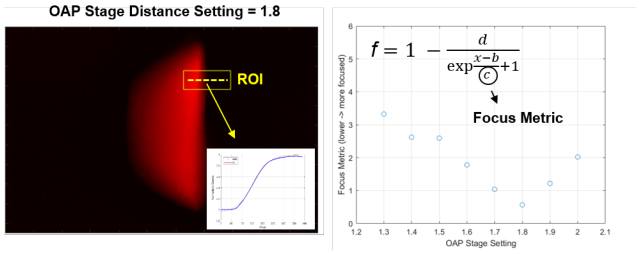

Figure 3: *Left*: Sample image observed at the optimal OAP distance taken with a lamp at the input of the monochromator. The inset shows a sample profile and fit with a Fermi function in the region of interest (ROI). *Right*: Dependence of focus metric on OAP distance setting. The fit function and the definition of this metric are shown.

was determined and used as the optimal position for instrument-level testing. Fig 3 shows an example of a focused image, sample profile, and fit for determining the distance of greatest contrast. The dependence of contrast on the OAP distance setting in the right figure shows 1.8 inches as the optimal distance setting, which corresponds to a distance of 9 inches from the output slit of the monochromator as expected.

The other key change to the optical setup was introducing coupling optics in front of the reference detector. A germanium lens couples the light onto the 1 mm x 1 mm HgCdTe detector instead of just using the bare detector. Our results shows the improvement in stability as the standard deviation averaged at each wavelength decreases even with a shorter lock-in amplifier time constant (3 seconds) than used in TIPCE (10 seconds) (Fig. 6). The consistency in these measurements showed negligible fluctuations in blackbody signal. Note that the transmission of the germanium lens is incorporated into the RSR calculation and its uncertainty incorporated into the uncertainty budget (discussed later).

4. INSTRUMENT-LEVEL RESULTS

Figure 4 (a) shows a preliminary operational version of TIRS-2 RSRs derived with instrument-level testing data; the in-band detector-level RSRs from each channel are averaged across all detector array locations. Figure 4 (b) shows an example from one location showing the expected (94 nm) dispersion corresponding to the slit width. This behavior is evidence of the improved alignment and/or collimation relative to the TIPCE measurements, since this behavior was not observed previously. Other evidence of the improvements in the measurement are shown in the RSR consistency in the along-slit direction, the higher SNR, and lower HgCdTe detector variability compared to TIPCE measurements as shown in Figures 5 and 6. These are reflected in the spectral response uncertainty budget.

The preliminary uncertainty budget is shown in terms of contributions to effective spectral radiance assuming blackbody spectra observations. The spectral response uncertainty per-detector indicates the quality of the measurement setup and procedures. This includes HgCdTe signal uncertainty, monochromator wavelength uncertainty, and TIRS-2 noise. We were not provided uncertainty contributions for the reflectance/transmittance spectra of the optical components or HgCdTe response, but we estimated the uncertainty using 10% of their maximum change within the chan-

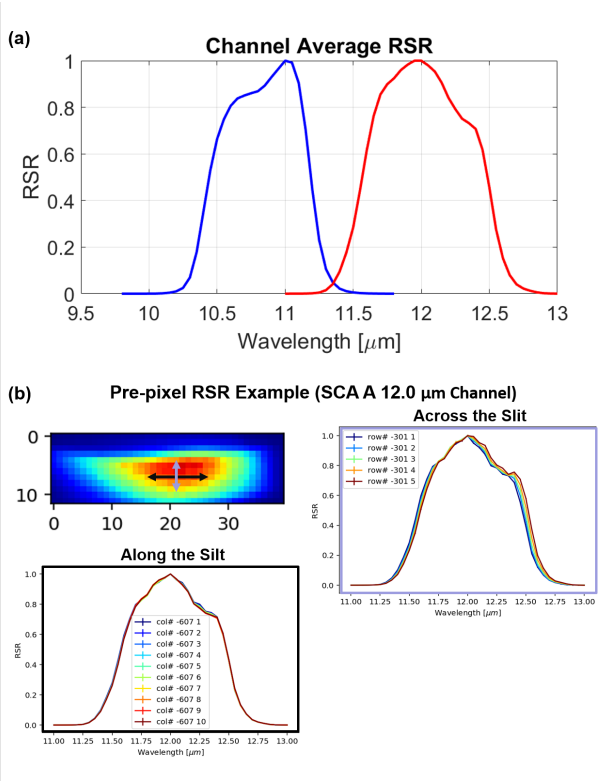

Figure 4: (a) Average RSR over all SCAs obtained from instrument-level testing. (b) Per-detector RSR example from SCA A showing the dispersion across the slit image in the vertical direction and no dispersion in the horizontal direction.

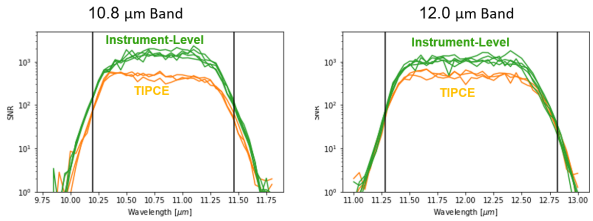

Figure 5: The per-pixel signal to noise ratio (SNR) results from instrument-level and TIPCE (sub-assembly-level) testing for each TIRS-2 band. The vertical lines denote the in-band region

nels. The wavelength calibration validation using three reference lines of a NIST standard reference material 1921B showed a negligible bias. The main source of wavelength uncertainty, however, is derived from the uncertainty in the wavelength position on the TIRS-2 image, which is a couple of TIRS-2 pixels or 20 nm (Fig. 7). The TIRS-2 noise term is calculated as the standard deviation of the mean for a typical pixel over its samples calculated per wavelength. We will include reproducibility when we repeat the measurement during the second instrument-level testing campaign this summer. Incorporating the RSR non-uniformity across locations gives the uncertainty introduced by using an average uncertainty per band to represent all detectors as is planned opera-

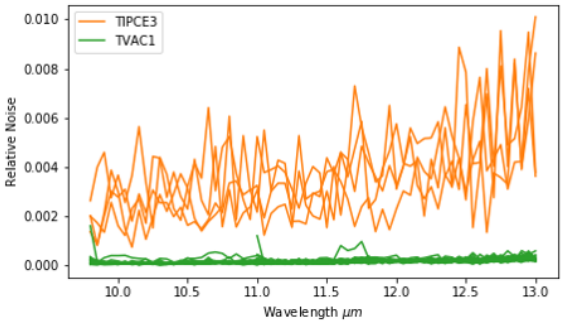

Figure 6: The variability (standard deviation) of HgCdTe detector measurements during TIPCE and instrument-level (TVAC) testing

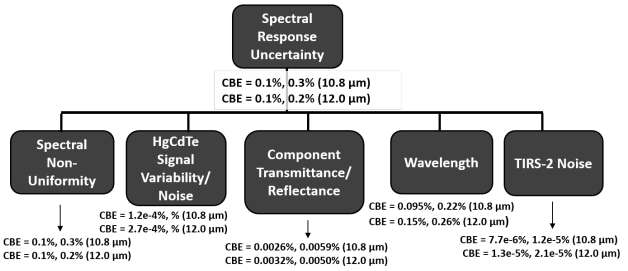

Figure 7: TIRS-2 spectral response uncertainty budget. The first number denotes uncertainty contribution assuming a scene brightness temperature of 260-330 K temperature range, and the second assumes a 240-260 K and 330-360 K scene. Note that the spectral response uncertainty includes spectral non-uniformity contributions across the detector arrays.

tionally. This is the dominant contribution to the spectral uncertainty. In the context of the overall radiometric uncertainty, the spectral uncertainty is fairly small. The dominant uncertainty contribution is expected to be from stray light effects (or out-of-field system scattered light) at 0.57% and 0.83%, for typical scene radiance and cold/hot scenes, respectively, although these are significantly reduced from TIRS on-board Landsat 8 as discussed in Ref. [7, 8]. A full discussion of the radiometric uncertainty is outside the scope of this paper but our analysis shows that TIRS-2 is expected to meet its radiometric uncertainty requirements of 2% and 4% (at typical and hot/cold temperature scenes, respectively).

5. CONCLUSIONS

The TIRS-2 instrument-level spectral response results show reduced uncertainty over our initial phase of pre-launch spectral testing. The setup improvements – a longer focal length off axis mirror for monochromator output collimation and an improved collimation methodology – increased system transmission and produced the expected wavelength dispersion behavior across the image of the monochromator slit. Coupling efficiency to the reference detector was increased to improve its stability. The instrument-level test generated a preliminary version of the RSRs expected to be used operationally due to its low uncertainties. The spectral test is part of a comprehensive pre-launch test plan to ensure that TIRS-2 will meet its performance requirements.

6. ACKNOWLEDGMENTS

The Authors thank Raviv Levy and Dr. Matthew Montanaro for helpful discussions and Jefferey Love for software support.

7. REFERENCES

[1] Dennis C. Reuter, Cathleen M. Richardson, Fernando A. Pellerano, James R. Irons, Richard G. Allen, Martha Anderson, Murzy D. Jhabvala, Allen W. Lunsford, Matthew Montanaro, Ramsey L. Smith, Zelalem Tesfaye, and Kurtis J. Thome, "The Thermal Infrared Sensor (TIRS) on Landsat 8: Design overview and pre-launch characterization," *Remote Sensing*, vol. 7, no. 1, pp. 1135–1153, 2015.

[2] James R. Irons, John L. Dwyer, and Julia A. Barsi, "The next Landsat satellite: The Landsat data continuity mission," *Remote Sensing of Environment*, vol. 122, pp. 11 – 21, 2012, Landsat Legacy Special Issue.

[3] J. H. Hair, D. C. Reuter, S. L. Tonn, J. McCorkel, A. A. Simon, M. Djam, D. Alexander, K. Ballou, R. Barclay, P. Coulter, M. Edick, B. Efremova, P. Finneran, J. Florez, S. Graham, K. Harbert, D. Hewitt, M. Hickey, S. Hicks, W. Hoge, M. Jhabvala, C. Lilly, A. Lunsford, L. Mann, C. Masters, M. Montanaro, T. Muench, V. Otero, F. Parong, A. Pearlman, J. Penn, D. Vigneau, and B. Wenny, "Landsat 9 thermal infrared sensor 2 architecture and design," in *IGARSS 2018 - 2018 IEEE International Geoscience and Remote Sensing Symposium*, July 2018, pp. 8841–8844.

[4] Xiaolei Yu, Xulin Guo, and Zhaocong Wu, "Land surface temperature retrieval from Landsat 8 TIRS—comparison between radiative transfer equation-based method, split window algorithm and single channel method," *Remote Sensing*, vol. 6, no. 10, pp. 9829–9852, 2014.

[5] M. Jhabvala, D. Reuter, K. Choi, C. Jhabvala, and M. Sundaram, "QWIP-based Thermal Infrared Sensor for the Landsat data continuity mission," *Infrared Physics & Technology*, vol. 52, no. 6, pp. 424 – 429, 2009, Proceedings of the International Conference on Quantum Structure Infrared Photodetectors (QSIP) 2009.

[6] B. Efremova, A. J. Pearlman, J. McCorkel, M. Montanaro, M. Hickey, A. Lunsford, and D. Reuter, "Landsat 9 Thermal Infrared Sensor 2 subsystem-level spectral test results," in *IGARSS 2018 - 2018 IEEE International Geoscience and Remote Sensing Symposium*, July 2018, pp. 8849–8852.

[7] Matthew Montanaro, Aaron Gerace, Allen Lunsford, and Dennis Reuter, "Stray light artifacts in imagery from the Landsat 8 Thermal Infrared Sensor," *Remote Sensing*, vol. 6, no. 11, pp. 10435–10456, 2014.

[8] M. Montanaro, J. McCorkel, J. Tveekrem, J. Stauder, A. Lunsford, E. Mentzell, J. Hair, and D. Reuter, "Landsat 9 Thermal Infrared Sensor 2 preliminary stray light assessment," in *IGARSS 2018 - 2018 IEEE International Geoscience and Remote Sensing Symposium*, July 2018, pp. 8853–8856.